Nat Hazards
DOI 10.1007/s11069-006-9105-y

ORIGINAL PAPER

Vulnerability assessment of rainfall-induced debris flows in Taiwan

George Y. Lu · Long S. Chiu · David W. Wong

Received: 20 September 2006 / Accepted: 28 December 2006

Abstract A GIS-based decision support system, which incorporates local topographic and rainfall effects on debris flow vulnerability is developed. Rainfall at a scale compatible with the digital elevation model resolution is obtained using a neural network with a wind-induced topographic effect and rainfall derived from satellite rain estimates and an adaptive inverse distance weight method (WTNN). The technique is tested using data collected during the passage of typhoon Tori-Ji on July 2001 over central Taiwan. Numerous debris flows triggered by the typhoon were used as control for the study. Our results show that the WTNN technique outperforms other interpolation techniques including adaptive inversed distance weight (AIDW), simple kriging (SK), co-kriging, and multiple linear regression using gauge, and topographic parameters. Multiple remotely-sensed, fuzzy-based debris-flow susceptibility parameters are used to describe the characteristics of watersheds. Non-linear, multi-variant regressions using the WTNN derived rainfall and topography factors are derived using self-organizing maps (SOM) for the debris flow vulnerability assessment. An index of vulnerability representing the degrees of hazard is implemented in a GIS-based decision support system by which a decision maker can assess debris flow vulnerability.

Keywords Debris flow · Spatial interpolation · Susceptibility · Vulnerability assessment · Decision support system · Satellite rainfall

G. Y. Lu (✉) · L. S. Chiu · D. W. Wong
Department of Earth Systems and GeoInformation Sciences, College of Science, George Mason University, Fairfax, VA 22030, USA
e-mail: glu@gmu.edu

L. S. Chiu
NASA/Goddard Space Flight Center, Data and Information Services Center, Greenbelt, MD 20771, USA

1 Introduction

Landslides are serious hazards common to many countries. While single-slope scale landslides cause damages in limited areas, wide-mountainous scale landslides, which move rapidly and occur mostly in mountainous areas, can cause significant fatalities and property damage. For example, the landslide that occurred on January 10, 2005 in the community of La Conchita in Ventura County, California killed 10 people and destroyed or seriously damaged 36 houses. Thousands of people died in the Leyte province of the Philippines on February 16, 2006 because of a massive debris flow event triggered by heavy rainfall. Globally, landslides cause billions of dollars in damages and thousands of deaths and injuries each year. A recent world disaster report by the International Federation of the Red Cross and Red Crescent Societies (2001) shows that flooding, avalanches, and landslides account for 42% of global incidence of natural disasters. In countries like Japan, India, Italy, Taiwan, and USA, the average yearly economic losses due to landslides amount to billions of US dollars. (Metternicht et al. 2005) In countries like Canada, Nepal and Sweden, the losses are in the millions (Metternicht et al. 2005).

A debris flow is usually triggered by heavy rainfall over mountainous areas. It is made up of mud, soils, gravels, rocks, and water. Solids or soils on steep slopes slide downward due to weathering processes and mechanical influence such as gravity or earthquake. Heavy rainfall facilitates this process by increasing pore water pressure, seepage force, and reducing effective stress of soils (normal stress carried by soil particles at the points of contact). Casagrande (1936) explained this mobilization as follows: if a dense soil is continually sheared, it will dilate and eventually attain a critical-state porosity. Loose soils will contract to reach the critical-state porosity. In both cases, the effective stress of soils can be regarded as Bingham viscoplastic material that denotes transition between solid-like and liquid-like behavior (Gabet and Mudd 2005). Hillslope materials can be mobilized by heavy rainfall and brought downstream along gullies with high flow velocity in the form of debris flows. Debris flows are more dangerous than floods because they typically carry large boulders and debris that can impact and destroy structures in their path. They can also dam channels and cause water to flood into areas that are not normally accessible by floodwater (Jan 2000).

Debris flows are closely related to topography and heavy rainfall (Lin and Jeng 2000; Lin et al. 2003; Tseng 2004; Wen and Aydin 2005). The goal of this research is to assess debris flow vulnerability based on these two factors at same geographic locations. A number of spatial interpolation techniques are examined for rainfall estimation. These techniques include inverse distance weighting method (IDW), adaptive inverse distance weighting method (AIDW) and kriging of existing gauge network, co-kriging and multiple linear regression (MLR) of gauge, and topographic parameters.

Local interaction between wind flow and topography can have a large effect on the local rainfall. The wind-topography interaction on rainfall is examined using a Wind-Topography neural network (WTNN). The local rainfall and multiple topographical factors are integrated into a debris flow vulnerability assessment model. Results of this research can be further developed into a more user-friendly GIS decision support system to facilitate hazard mitigation.

The success of vulnerability assessment of debris flow is mostly governed by the accuracy of rainfall measurements (Tseng 2004; Huang 2002). There are limitations in, and controversies among, different rainfall estimation methods. Lin et al. (2003) and Cheng et al. (2005) estimated the amount of rainfall that triggered a debris flow event based on the

rainfall amount recorded by the nearest rain gauge. Obviously, this assumption is not persuasive. Tseng (2004) applied inverse distance weighting (IDW) method to improve rainfall estimates. This method was first proposed by the US National Weather Service in 1972 and has been extensively applied to rainfall estimation. It is fast and easy to compute. However, IDW is in general considered to be inferior to other stochastic approaches such as kriging, co-kriging or, linear regression methods (Goovaerts 2000; Dingman 2002).

To avoid costly and extensive field trips to maintain and gather data from gauges, especially in mountainous areas, remote sensing data provide a nice alternative method for acquiring rainfall data. Tseng (2004) collected historical data of debris flows over the central part of Taiwan and proposed fuzzy-based equations with input variables that are obtained from high-resolution digital elevation model and high-resolution satellite imagery.

Existing vulnerability assessment methods for debris flows are either based on threshold values with arbitrary numbers (Lin et al. 2002) or principal component analysis (Jakob and Weatherly 2003). Evidence shows that self-organizing maps (SOM) may perform better (Giraudel and Lek 2001; Leflaive et al. 2005). This research evaluates the performance of SOM, which has been proven to be an effective tool in dealing with classifying groups (Chon et al. 1996; Levine et al. 1996).

In this paper, we review existing debris flow research and traditional spatial interpolation techniques for rainfall interpolation. Next, we describe spatial interpolation techniques for rainfall and methods to obtain multiple topographical factors. Lastly, we describe and discuss our results on estimation of optimal rainfall interpolation and the use of multiple topographical factors in vulnerability assessment of watersheds in central Taiwan.

2 Literature review

2.1 Landslide analysis

Studies on landslides can be generally divided into two categories: the single-slope scale and regional scale analyses. Studies on single-slope scales focus on evaluating the possibility of landslide occurrence for individual slopes. Studies on a regional scale mainly deal with multiple or massive landslides, including debris flows. There are well-developed approaches to assess landslide vulnerability. These approaches can be classified into four broad categories (Ermini et al. 2005): (a) landslide inventories; (b) heuristic methods; (c) deterministic approaches and (d) statistical analyses.

The landslide inventories and heuristic methods are typically based on field and remote sensing investigation to produce landslide hazard maps. These two methods suffer significantly from unreliable quality control due to a high-level of subjectivity and the varying experiences of the investigators. (Ermini et al. 2005) Deterministic methods, which are widely applied in geotechnical engineering, aim at evaluating the likelihood of landslides based on factor of safety analysis. The factor of safety is based on geotechnical data which include soil properties (i.e., soil unit weight, internal friction, cohesion, pore pressure) and geomorphic properties (i.e., slope angle, slope height, depth of soil layer, and groundwater seepage) (Taylor 1937; Bishop 1955; Bishop and Morgenstern 1960). In general, deterministic approaches are reliable only when failure mechanisms are fully understood and quality geotechnical data are available. For most cases, especially in mountainous areas, the in situ sampling and laboratory testing of these data is costly and sometimes impractical.

To circumvent the difficulties of acquiring in situ data, remotely-sensed data and Geographic information system (GIS) are becoming more used (Clerici et al. 2002; Cheng 2003; Jakob and Weatherly 2003; Tseng 2004; Ayalew and Yamagishi 2005, Cheng et al. 2005, Luino 2005; Malet et al. 2005; Shakoor and Smithmyer 2005; Wen and Aydin 2005). GIS provides a platform for spatial data inventory and manipulation. Remote sensing data can be transformed into thematic layers and processed by grid-based computation with other gird format data, such as digital elevation model (DEM), in a GIS environment.

2.2 Debris flows

Debris flows are mixtures of water, air, clay minerals, and granular solids with a wide variety of sizes. Each component affects the properties of debris flows. Debris flows can travel with high velocity (tens of meters per second) on slopes ranging from 6° to 30°. Simple, idealized theoretical models have been developed to analyze debris flows according to observations of small experimental flows and natural debris flow deposits (Johnson 1965). Sidle et al. (1985) identified five natural factors that are most influential to debris flows:

1. Soil/rock properties, especially the hydrologic and mineralogical conditions that affect engineering soil/rock behavior and strength properties of colluvium;
2. Geomorphology, including the geologic and tectonic setting, slope gradient, and shape of watersheds;
3. Surface, subsurface, and rainfall hydrology;
4. Vegetative cover, including the reinforcing effect of root systems;
5. Seismicity, especially the potential for liquification of marginally stable soils on steep slopes.

Hsu and Lu (2004) showed that in Taiwan, debris flows take place on converged convex slopes that usually have a bowl-shaped appearance, with a constriction of 4–6 m wide below the sliding area. The scale of the slide and the size of the sliding area are all significantly greater than that of the other slope movements. His study also stressed that watershed size is significantly related to debris flows. Liu (2001) analyzed factors that contribute to debris flows in central part of Taiwan by principal component analysis (PCA). Factors are watershed area, length of stream, shape factor, vegetative cover, and slope of stream. His results show that watershed area, length of stream and vegetative cover significantly influence debris flows.

Lunio (2005) studied three debris flow cases in northern Italy: the July 1987 event in Valtellina, the November 1994 event in the Tanaro river basin, and the October 2000 event in the Aosta Valley. The region is geomorphologically heterogeneous with high mountains, wide valleys, gentle hills, and a large plain forming a highly varied landscape that influences climate in the area. These characteristics are very similar to our study area, the central part of Taiwan. The results showed that the quantity of debris flows triggered by rainfall was related not only to morphological and geological characteristics, but also to the intensity and spatial distribution of rainfall.

This paper considers the above debris flow characteristics and uses them as input variables for vulnerability assessment. The detailed discussions of these input variables will be on Sect. 3.1.2.

2.3 Rainfall analyses

Heavy rainfall is one of the factors that will initiate the instability processes for debris flows. It causes soil saturation and a rise in pore-water pressure (Clerici et al. 2002). In un-gauged watersheds, methods to estimate rainfall using rain gauges in adjacent watersheds are necessary. The Thiessen polygon method involves assigning the rainfall at each location to the closest gauge measurement for subregions of polygons (Thiessen 1911). In 1972, the US National Weather Service proposed the inverse distance weight method (IDW) by using weights inversely proportional to the squared distance between the rain gauge and an un-gauged location (Dingman 2002). The IDW method is fast and easy to compute, and therefore, widely used. The IDW is usually modified by a constant power, or a distance-decay parameter, to reflect the diminishing relationship with increasing distance. Recognizing the potential of varying distance-decay relationship over a study area, the parameter may vary according to the spatial pattern of the sampled points in the neighborhood. An adaptive approach suggests that the distance-decay parameter is a function of the point pattern of the neighborhood. This adaptive spatial interpolation method based upon IDW is called the adaptive inversed distance weighting method (AIDW).

Geostatistical approaches such as kriging are increasingly preferred over distance weighting methods because they establish a best linear unbiased estimate (BLUE) by minimizing the variance of attributes of neighborhood sample points. Geostatistical approaches have been found to provide better estimations than other deterministic methods, such as IDW (Tabios and Salas 1985; Philips et al. 1992). Lebel et al. (1987) compared Thesisen's polygon, spline fit, and kriging approaches for estimating areal precipitation for durations of 1–24 h. Among all methods examined, kriging was judged to be the most accurate at all gauge densities and for all durations. Borga and Vizzaccaro (1997) compared kriging with the multi-quadratic method using various gauge densities on Monte Grande Hill, Italy. Their results suggested that kriging is remarkably more accurate at lower densities (less than 0.022 gauges km^{-2}) in a 30×30 km^2 study area. However, Dirks et al. (1998) applied kriging, inverse distance weight, Thiessen's polygon, and areal-mean methods to estimate rainfall from a network of 13 rain gauges for a small study area of 35 km^2 on Norfolk Island. He showed that kriging provided no significant improvement over other computationally simpler methods, such as IDW, and recommended that the IDW method was adequate for spatially dense networks. Kriging did not improve on the interpolation over IDW because the network semivariogram, which provides information of the structure of spatial variability, did not reach the span of this particular network. In other words, the unsatisfactory result of kriging was due to the absence of prominent spatial structure that was reflected in a poorly fitted semivariogram (Isaaks and Srivastava 1989).

Kyriakidis et al. (2001) developed a kriging-based spatial interpolation technique to estimate rainfall. Unlike others, Kyriakidis et al. adopted the concept of simple kriging that required a regional mean for rainfall amount and local variability. The local variability is defined by the residuals of the regional mean and sampled data. In most cases, regional mean is not easy to obtain. However, Kyriakidis et al. (2001) assumed the regression-based result as the regional mean and used kriging to interpolate the local variability. Then the interpolated local variability was added to the regional mean to complete the spatial interpolation. Kyriakidis et al. (2001) also addressed the atmospheric variables that are typically available at a very coarse resolution, but provide a general coarse-scale state of the atmosphere, which is expected to bear some relevance to

observed precipitation at the local scale. However, coarse-scale data may fail to reflect local variability. As one can expect, results of the interpolation are with coarse resolution because the results are constrained by the relatively low resolution of the input meteorological variables. Therefore, those results may not be appropriate for estimating rainfall at the local scale for debris flows susceptibility analysis. To overcome this limitation, this study exploits the use of space-borne remote sensing rainfall data as the regional mean rainfall, and adopts interpolated results by AIDW as local variability to fit Kyriakidis' model.

The orographic effect causes air to be lifted or lowered vertically, and condensation due to adiabatic cooling or heating tends to modify precipitation. Correlation between rainfall and elevation ranges from 0.33 to 0.83 over the Algarve's mountains in the southern most region of Portugal (Goovaerts 2000). Hevesi et al. (1992) reported a significant correlation ($R = 0.75$) between average annual precipitation and elevation recorded at 62 stations in Nevada and southern California.

To incorporate elevation information for rainfall estimation, Daly et al. (1994) proposed the Precipitation-elevation Regression on Independent Slopes Model (PRISM), which estimates rainfall at a DEM grid cell by establishing a regression of rainfall versus elevation through moving windows. The results are better than that of kriging, de-trended kriging, and co-kriging (with DEM). Daly et al. (1994) pointed out two limitations of PRISM. For regional applications in mountainous terrain, PRISM performs consistently well only when the DEM has a resolution better than approximately 6 km. Due to the moving window technique that smoothes topography to increase the correlation between precipitation and elevation, PRISM has limited capability over rugged terrains. Those two limitations illustrated that PRISM is more appropriate for larger geographical coverage or global rainfall studies.

Goovaerts (2000) reviewed the use of co-kriging to incorporate elevation into the mapping of rainfall. His results, however, show that the interpolation errors from co-kriging are larger than those of kriging. The reason of the poor performance is that if the primary and secondary variables are co-located and the auto- and cross-variograms are proportional to the same basic model, then the co-kriging method will not improve the estimation (Isaaks and Srivastava 1989), i.e., benefit of co-kriging is marginal if the correlation between rainfall and elevation (or other environmental description) is small. Isaaks and Srivastava (1989) suggested that co-kriging rainfall and elevation does not seem to be a good method for rainfall estimation.

Orographic rainfall is modified by the surface wind. In general, there is rainfall enhancement on the windward side and a decrease in rainfall on the leeward side of a mountain. The wind factor has been considered by a number of researchers (Kyriakidis et al. 2001; Bindlish and Barros 2000; Prudhomme 1999). Prudhomme (1999) suggested that the variables aligned to the prevailing wind direction are the most significant for estimating rainfall. Kyriakidis et al. (2001) included wind information as a predictor to estimate rainfall. Besides regression models, artificial neural networks (ANN) were used in rainfall analysis by treating wind information as one of the input variables (Navone and Ceccatto 1994; Hsu et al. 1997; Luk et al. 2001). Ramirez (2005) applied ANN to construct a nonlinear map between wind derived from a regional ETA model and surface rainfall data in the region of Saõ Paulo State, Brazil. Comparison with a multiple linear regression model showed better results than ANN. In this paper, we improved on Ramirez's work by proposing a wind-topographic model using ANN. Inputs to the ANN are rainfall and the combined effect of wind and topography.

2.4 Debris flow vulnerability

Since debris flow is a complex phenomenon in nature, a versatile debris flow vulnerability model should be able to fully accommodate their complicated mechanisms. This paper aims at developing a hazard assessment model with input variables that can be derived easily and efficiently with low cost. Hürlimann (2006) suggested a series of multidisciplinary approaches for debris flow hazard assessment. There were three steps in the assessment: geomorphologic and geologic analysis, runout analysis, and hazard zonation. An exhaustive field surveys and interpretation of aerial photographs and the study of historic data are required to finish the first step. Input parameters to the runout analysis included topographic profile, channel shape and width, rheologic parameters, and the initial volume. Two parameters for the rheologic model are the dry friction coefficient and the Chezy-like turbulent friction term. A hazard matrix can be used to analyze these parameters to assist the process of hazard zonation. Generally speaking, Hürlimann's method does not fit as an ideal hazard assessment model because it relies heavily on field surveys and laboratory examination. The hazard matrix is also too imprecise to define degrees of hazard by just assigning threshold values.

On the broader issue of landslide assessment, Komac (2006) created a mass landslide susceptibility model based on statistical relationships and concluded that multivariate statistics are most effective in developing a mass landslide susceptibility model. Ayalew and Yamagishi (2005) compared two vulnerability assessment methods: the analytical hierarchy process (AHP) method and the logistic regression method. The differences between AHP and logistic regression are relatively minor when the number of susceptibility classes is small. However, when the number of susceptibility classes is large, the logistic regression map tends to outperform AHP. Besides multivariate statistical methods, artificial neural networks are also used in vulnerability assessment. ANN tends to outperform multivariate statistics (Pérez-Magariño 2004; Giraudel and Lek 2001; Leflaive et al. 2005). Gómez and Kavzoglu (2005) used land cover, slope angle, slope aspect, elevation, topographic wetness index, lineaments, and soil types as input to an ANN to access landslide vulnerability zonation in the Jabonosa river basin, Venezuela. Their results show a 90% overall accuracy using the ANN technique. Ermini et al. (2005) utilized ANN with input variables including lithology, land cover, slope angle, curvature, and up-slope contribution area, and found prediction made by ANN were satisfactory in the Riomaggiore catchment area, Italy. Since the applications of using ANN to assess landslide events seem very promising in previous studies, this paper will evaluate the effectiveness of using ANN in debris flow assessment.

Specifically, we will use self-organizing maps, a type of ANN, to conduct a debris flow vulnerability assessment in central part of Taiwan. We will improve on Ramirez's work by proposing a wind-topographic model using ANN with triggering rainfall and debris flow susceptibility factors as inputs. The methodology, study area, and data used are described below.

3 Methodology, study area, and data

3.1 Methodology

The methodology can be divided into three parts: (1) triggering rainfall, (2) debris flow susceptibility factors, and (3) vulnerability assessment

3.1.1 Triggering rainfall

We assume that debris flows are triggered by rain falling on a particular DEM grid cell. The amount of rainfall is estimated by spatial interpolation made from nearby rain-gauge data. Three spatial interpolation techniques, adaptive inverse distance weight method (AIDW), simple kriging method (SK), and wind-topography neural network method (WTNN) were tested. AIDW improves inverse distance weight (IDW) method by regarding distance decay parameters as variant instead of constant; SK incorporates remote sensing information as regional mean and interpolated rainfall data as the local variant; WTNN is based upon a back propagation neural network that provides a platform for the interactions among wind, topography, and rainfall.

Adaptive inverse distance weight method (AIDW). The IDW is a straight-forward and computationally simple method. It has been regarded as one of the standard spatial interpolation procedures in geographic information science (Burrough and McDonnell 1998; Longley et al. 2001) and has been implemented in many GIS software packages. Formally, the IDW method is used to estimate the rainfall value ($\hat{y}$) at location S_0, given the observed rainfall values y in sampled locations S_i in the following manner:

$$\hat{y}(S_0) = \sum_{i=1}^{n} \lambda_i y(S_i) \tag{1}$$

Essentially, the estimated value at S_0 is a linear combination of weights (λ_i) and the observed y values at S_i where (λ_i) is often defined as

$$\lambda_i = d_{0i}^{-\alpha} / \sum_{i}^{n} d_{0i}^{-\alpha} \tag{2}$$

where

$$\sum_{i}^{n} \lambda_i = 1$$

In Eq. 2, the numerator is the inverse of distance (d) between S_0 and S_i raised to a power α, and the denominator is the sum of all inverse distance weights for all locations so that the sum of λ_i for an unsampled point will be unity. The α parameter specifies the geometric functional form of the weight, such that if α is larger than 1, the so-called distance decay effect will be more than proportional to a given increase in distance. Small α tends to average S_i, whereas large α tends to give larger weight to nearer points and increasingly ignores points further away. When $\alpha \to 0$

$$\begin{aligned} \lambda_i &= 1/n \\ \hat{y}(S_0) &= \sum_{i=1}^{n} \lambda_i y(S_i) \\ &= \sum_{i=1}^{n} \frac{1}{n} y(S_i) \end{aligned} \tag{3}$$

When $\alpha \to \infty$

$$\lambda_i = \begin{cases} I & i = j \quad (L_j = \min\{L_i\}) \\ 0 & i \neq j \end{cases}$$

$$\hat{y}(S_0) = \sum_{i=1}^{n} \lambda_i y(S_i) = y(S_j) \tag{4}$$

According to the First Law of Geography (Tobler 1970), ''everything is related to everything else, but near things are more related than distant things.'' The main objective of AIDW is to use a small α to average the clustering points with similar attributes (Eq. 3), and assign a large α for neighboring points in a dispersed pattern (Eq. 4).

To guide the selection of α based upon the clustering pattern, we rely on concepts of nearest neighbor statistics (Wong and Lee 2005) The expected nearest neighbor distance for a random pattern can be calculated as

$$r_{\text{exp}} = 1/(2(n/A)^{0.5}) \tag{5}$$

where n is the number of total points in the study area, and A is the area of the study region.

With both the observed and the expected nearest neighbor distances, the nearest neighbor statistic, R, can be expressed as:

$$R = r_{\text{observed}}/r_{\text{expected}} \tag{6}$$

The smaller the R, the more clustered the pattern, and vice versa.

Here, r_{observed} is calculated for the set of five points closest to the unsampled location. The expected nearest neighbor distance for a random pattern (r_{expected}) is a constant over the entire area, therefore, the R value is governed by the observed average nearest neighbor distance, r_{observed}.

Instead of using R value, we normalize the R value into a μ_R value, $0 \leq \mu_R \leq 1$, where:

$$\mu_R = \begin{cases} 0, & R(S_0) < R_{\min} \\ 0.5 + 0.5\sin(\pi/R_{\max})(R(S_0) - R_{\min}), & R_{\min} \leq R(S_0) \leq R_{\max} \\ 1, & R_{\max} < R(S_0) \end{cases} \tag{7}$$

$R_{\min}$ refers to a local nearest neighbor statistic value below which μ_R is set to zero. $R_{\max}$ refers to a local nearest neighbor statistic value above which μ_R is set to one. Empirically, $R_{\min}$ and $R_{\max}$ can be set to the minimum and maximum, respectively, of $R(S_0)$ for all locations of S_0, the sampled points. $R_{\max}$ and $R_{\min}$ are determined by the global statistics of the entire sample of points.

We evenly divided $\{\mu_R | \ \mu_R(0,1)\}$ into five categories (0.1, 0.3, 0.5, 0.7, 0.9) and assigned a distance decay value to each category. The extreme clustering ($\mu_R = 0.1$) and dispersing ($\mu_R = 0.9$) categories were assigned the minimum and maximum distance decay values, whereas for the others (μ_R equals to 0.3, 0.5 and 0.7) the distance decay values are linearly selected between the maximum and minimum distance decay values. The triangular weighting function (Fig. 1) determines the distance decay parameters. The determination is based on linear interpolation. To illustrate the concept, if $R(S_0)$ for an unsampled location is 0.8, the corresponding μ_R is 0.35 from Eq. 7. According to the

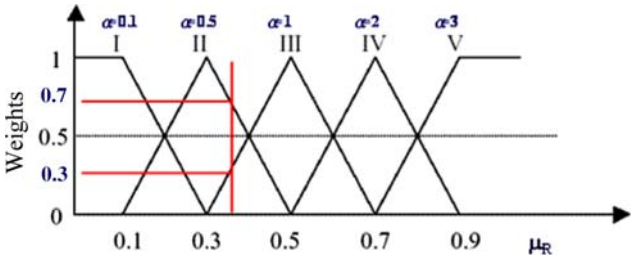

Fig. 1 Triangular Weighting Function for different degrees of adaptive distance-decay parameter

triangular weighting function in Fig. 1, a μ_R of 0.35 corresponds to two points (0.3 for category III and 0.7 for category II). These values are used as the weights to be applied to the corresponding α assigned to the categories to derive the final α value. As a result, the final α is $(0.7 \times 0.5 + 0.3 \times 1) = 0.65$. Note that the sum of the two weights for any μ_R value is always 1. The values of α equal to 0.1, 0.5, 1, 2, and 3, respectively, are assigned to these categories after heuristically testing their applicability in this specific context.

Simple kriging method (SK). The simple kriging (SK) method uses rainfall values from satellite data as the regional means and adopts results of *AIDW* as the local variability. The detailed description of the procedure follows: First, random points are selected within a satellite pixel and then each point was assigned a value, $Z(u_\alpha)$ by using AIDW. The satellite remote sensing information is regarded as the local mean, $\hat{m}_{\mathrm{Sat}}$. The residuals of satellite remote sensing information and AIDW within a satellite pixel are obtained by subtracting $\hat{m}_{\mathrm{Sat}}$ from $Z(u_\alpha)$. To ensure that the residuals of $\hat{m}_{\mathrm{Sat}}$ and $Z(u_\alpha)$ are unbiased and variance minimized, ordinary kriging is used. The value of un-sampled locations within a satellite pixel can be expressed by

$$Z(u_0) = \hat{m}_{\mathrm{Sat}} + \sum_{\alpha=1}^{n} \lambda_\alpha^{\mathrm{OK}}(u_0)[Z(u_\alpha) - \hat{m}_{\mathrm{Sat}}]$$

$$\text{with} \sum_{\alpha=1}^{n} \lambda_\alpha^{\mathrm{OK}} = 1 \text{ and } \lambda_\alpha^{\mathrm{OK}} = \text{weights} \tag{8}$$

.

The objective of Eq. 8 is to find weights, $\lambda_\alpha^{\mathrm{OK}}$, that give an unbiased estimate $E[\{\Delta\hat{Z}_{\mathrm{OK}}(u_0) - \Delta Z(u_0)\}] = 0$ and variance$\hat{\sigma}^2_{\mathrm{OK}}(u_0)$, that is minimized by the Lagrange parameter Ψ_{OK}.

$$\hat{\sigma}^2_{\mathrm{OK}}(u_0) = \Psi_{\mathrm{OK}} - \gamma(0) + \sum_{\alpha=1}^{n} \lambda_\alpha^{\mathrm{OK}} \gamma(\Delta u_\alpha - \Delta u_0) \tag{9}$$

Wind-topography model. Two different estimators of the topographic exposure to the hypothetical wind flux are selected and modeled. Each of them is examined for eight different directions using an azimuthal step of 45° (N, NE, E, SE, S, SW, W and NW) as shown in Fig. 2 (Antonic and Legovic 1999). Since direction pairs that are 180 degree out of phase give identical results with opposite signs, only four directional statistics are needed for interpretation.

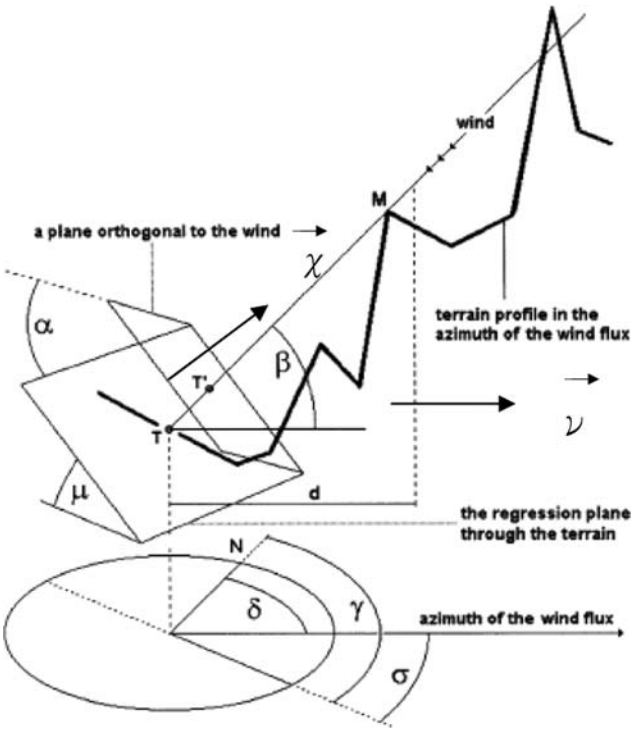

Fig. 2 Illustration of wind-topography model (after Antonic and Legovic 1999)

The first estimator, Asp, is the *relative aspect* (σ),which is the difference of angles between the azimuth angle of hypothetical wind flux, δ, and the terrain aspect, γ (see Fig. 2). The second estimator is the *terrain exposure toward the horizontal component of the wind flux,* Exp(0).It is defined as the cosine of the angle α, between the terrain orthogonal vector, χ, to the direction of the (hypothetically) horizontal wind flux, ν.

$$\mathrm{Exp}(0) = \cos\alpha = \frac{\vec{x} \bullet \vec{v}}{|\vec{x}|\,|\vec{v}|} \tag{10}$$

The second estimator Exp(0) can be computed from Eq. 11.

$$\mathrm{Exp}(0) = \cos\alpha = \cos(\mu)\sin(\beta) + \sin(\mu)\cos(\beta)\cos(\delta - \gamma) \tag{11}$$

where μ is the terrain slope and β is the elevation angle of wind flux. For the second estimator, if horizontal wind β = 0, then Eq. 11 can be rewritten as

$$\mathrm{Exp}(0) = \cos\alpha = \sin(\mu)\cos(\delta - \gamma) \tag{12}$$

These estimates are inputs to the wind-topographic model, which will be estimated by artificial neural networks (ANNs), a relatively versatile nonlinear modeling tool, to model wind and topography in relation to precipitation. The selected neural network model is back propagation neural network (BPNN), which has the ability to adjust weights

according to the residues of the predicted value and target value for each learning episode. Input variables are Asp (aspect), Exp(0), elevation (Z) and results from AIDW. The rain gauge data serve as the target values. By examining the difference between the target value and output values, BPNN can adjust weights according to the responses from the error term through its nonlinearly regressive behavior until the error is converged or acceptable.

Performance evaluation. The comparison between rain gauge data and interpolated rainfall value derived from different models are evaluated by root-mean-square error (RMSE) given by

$$\mathrm{RMSE} = \sqrt{\frac{1}{N_{\mathrm{vald}}}\sum_{i=1}^{N_{\mathrm{vald}}}(P_i - P*_i)^2} \tag{13}$$

where N_{vald} is the total number of validation points. P_i is the interpolated rainfall for the ith grid and $P * i$ is the corresponding ith observation. About 20% of the measurement points are kept for validation purposes. Then, $N_{\mathrm{vald}} = N \times 20\%$ where N is the number of total rain gauges. The *Percent Error*, PE (%), is defined by

$$\mathrm{PE}\ (\%) = \frac{\mathrm{RMSE}}{\frac{1}{N_{\mathrm{vald}}}\sum_{i=1}^{N_{\mathrm{vald}}} P*_i} times; 100(\%) \tag{14}$$

3.1.2 Debris flow susceptibility factors

At a watershed scale, certain factors are favorable to debris flows. The factors we considered are from Tseng (2004):

(1) Slope of hillslope. Slope of hillslope provides a gravitational field for mass transport and debris flow occurrence, and governs the behavior of debris flow movement (Tseng 2004).
(2) Vegetative cover. Loosened solids play an important role in providing material for debris flows. The colluvial materials and talus materials accumulated in gully areas are typically source areas for debris flows triggered by heavy rainfall. Debris flows are often initiated in scarred terrain (Jakob 2000) and are strongly related to vegetative cover.
(3) Area of watershed. Larger catchment areas receive larger amount of rainfall and yield more runoff. Therefore, the likelihood of debris flow occurrence increases in relation to the size of watershed (Vanacker et al. 2003; Hsu and Lu 2004).
(4) Soil type. Jiang (1998) classified seven soil types (meta-sandstone, shale, conglomerate, alluvium, sandstone, slate, sandstone, and shale) in central part of Taiwan. Each soil type is assigned a weight to represent the vulnerability to debris flows. The larger the weight, the more vulnerable to debris flow. Results show that sandstone and shale is most likely related to debris flow, whereas alluvium is least likely. The weights used for each soil type were alluvium (1.125), sandstone (1.625), conglomerate (2.125), slate (6.5), meta-sandstone (7.125), sandstone, and shale (10).

Tseng (2004) collected historical data for those watersheds that were vulnerable to debris flow in central Taiwan and proposed a fuzzy-logic-based equation for each topographic factor as follows.

$$N_1(S) = 1 - e^{-0.003S^2} \tag{15}$$

where S is the slope of hillslope in percentage, S = (Elev. at head of watershed − Elev. at downstream terminus of watershed)/Length of watershed

$$N_2(R) = 1 - e^{(-0.6R)} \tag{16}$$

where R is percentage of non-vegetation-covered area, R = (Watershed area − vegetation-covered area)/Watershed area

$$N_3(A) = \begin{cases} 0.02A, A \leq 50 \\ 1, A > 50 \end{cases}. \tag{17}$$

where A is watershed area in units of hectares,

$$N_4(W_i) = 0.11W_i - 0.11, \quad 1 < W_i \leq 10$$
$$W_i = 9\frac{X_i}{X_{\max}} + 1 \tag{18}$$

where W_i is the weighting of soil types, X_i is the frequency of soil type in a watershed, X_i= {meta-sandstone, shale, conglomerate, alluvium, sandstone, slate, sandstone and shale} and $X_{\max} = \max\{X_i\}$.

3.1.3 Vulnerability assessment

To prioritize watersheds for hazards mitigation, watersheds were classified according to the degree of hazard. In this study, an unsupervised training method in an artifical neural network (ANN), and the Kohonen's self organizing map (SOM) classifier, which divides the input space into a desired number of classes, were used for classification. The output from an SOM is topologically ordered in the sense that the nearby neurons in the output layer correspond to similar input. The Kohonen network's ability to transform the input relationships into spatial neighborhoods in the output neurons has been used for applications in areas such as classification, feature mapping, and feature extraction (Jain and Srinivasulu 2006). The neurons having similar characteristics were grouped in one single layer. For example, the neurons in an input layer received the input from an external source, and transmit the same information to a neuron in an adjacent layer, which could either be a hidden layer or an output layer. Each neuron in an ANN was also capable of comparing an input to a threshold value. The input vector presented to an ANN should be normalized between 0 and 1. The learning in the SOM was based on the concept of clustering of input data. SOM had the ability to assess the input patterns presented to the networks, organize itself to learn its own similarities based on the collective set of inputs, and categorized them into groups of similar patterns. For the classification of the input vectors, the clustering was meant to group of similar objects and separate dissimilar ones. The SOM training started by initializing the weight vector and normalized the input vectors. During the self-organization process, the cluster unit, whose weight vector most closely matched the input pattern, was chosen as the ''winner neuron.'' The winner neuron was selected based on competitive learning and similarity clustering. The minimum Euclidian distance was adopted as the similarity rule. The winner neuron and its

neighboring units updated their weights. The procedure is repeated by presenting all input vectors, and convergence is achieved by fine tuning the learning rate and the size of the neighborhood (Jain and Srinivasulu 2006).

The values of learning rate and neighborhood distance of 0.9 and 0.2 were employed in this study to achieve convergence. Initial weights were assigned using random numbers. Outputs are five categories of degrees of hazard.

3.2 Data and study area

The study area is located in central Taiwan, with a total area of 6,320 km^2 and rain gauge density of 0.006 gauges km^{-2}. After the Chi–Chi earthquake struck Taiwan in 1999, the number of landslides in this area increased from 7.1×10^6 m^2 (1996–1998) to 27.5×10^6 m^2 in 2001 (Lin et al. 2003). On July 29, 2001 typhoon Tora-Ji hit the study area with heavy rainfall, caused mass landslides, and caused high economic and human losses. A total of 1972 houses were destroyed, over six million US dollars losses, and caused 43 deaths, 113 people disappeared, and 32 injured. Hourly rain gauge measurements from 39 rain gauges maintained by the Taiwan Central Weather Bureau over the study area were collected. The distribution of the 39 gauges is shown in Fig. 3. We randomly selected 30 gauges for the spatial interpolation (training) process, and reserved the remaining 9 gauges for validation.

Satellite rainfall estimates were retrieved from the Tropical Rainfall Measuring Mission (TRMM) combined instrument 2B31 algorithm (Kummerow et al. 2000). TRMM is an international satellite designed to study rainfall systems and structures in the tropics and sub-tropics. The TRMM rain sensors include the first space-borne precipitation radar (PR), a TRMM Microwave Imager (TMI), and a Visible and Infrared Scanner (VIRS) (Kummerow et al. 2000). This paper adopts the TRMM 2B31 algorithm to produce the rainfall information, used as the local mean for the simple kriging (SK) method. The TRMM combined instrument algorithm (2B31) uses the PR measured radar reflectivities constrained by the microwave emissions measured by the TMI to produce the best TRMM sensor rain estimate (Kummerow et al. 2000). Additionally, the PR estimates are deemed more reliable and there is little bias between PR and TRMM Combined Instrument (TCI) estimates (e.g., Chiu et al. 2006a and b). The TCI has a ground resolution the same as that of PR, which is about 4 km at nadir.

A 1×1 km^2 DEM was obtained from HYDRO1k (http://www.edc.usgs.gov/products/elevation/gtopo30/hydro/index.html). HYDRO1k is developed by the U.S. Geological Survey's (USGS) EROS Data Center and provides consistent global coverage of topographically derived data sets. HYDRO1k provides a standard suite of geo-referenced data sets at a resolution of 1 km. Terrain slope and aspect are processed by ArcGIS, a popular GIS software package, with outputs at the same resolution.

In order to better define a rainfall event that triggers debris flows, this paper adopts the method used by Huang (2002). Huang's method defines the starting point of a typhoon event when more than 4 mm rainfall accumulation is measured, and the ending point of rainfall at the beginning of a 6-h duration when less than 4 mm rainfall accumulation is measured. Both adaptive inverse distance weight and wind-topography methods were used.

Since the TRMM Satellite path was not able to catch the peak rainfall event defined by Huang's method, we used the fly-over orbit that is closest to the debris flow event of interest (orbit number 21129 on 17:51:49 2001-07-29 to 19:23:08 2001-07-29). The rain gauge data within a 3 h envelope around the satellite passage time is used for the simple kriging method.

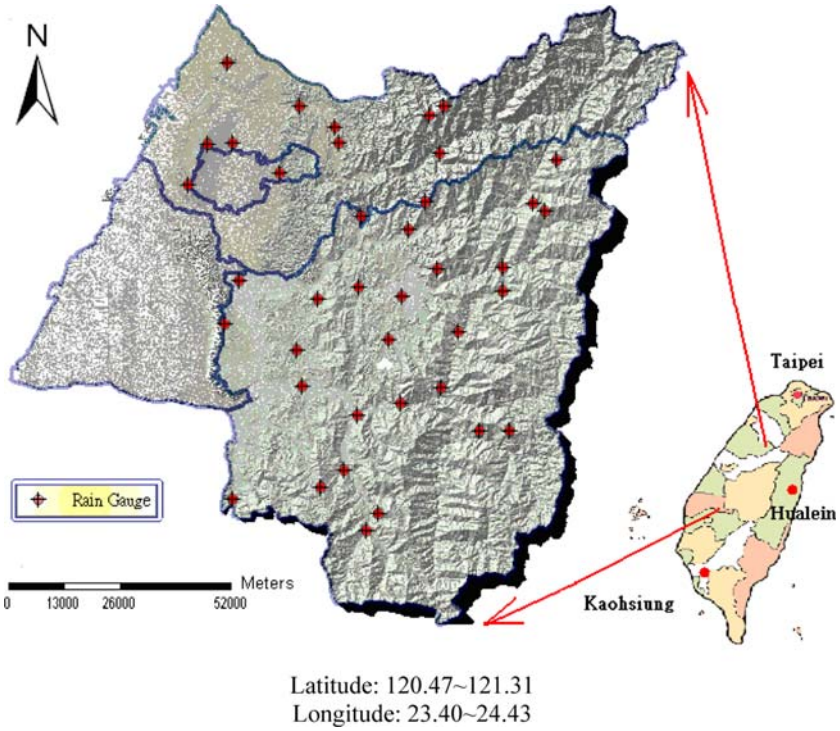

Fig. 3 Distribution of the 39 rain gauges in the central portion of Taiwan

There is no wind information at each gauge stations. However, both radiosonde stations in Nan-Too and Taichung show southeasterly winds during the typhoon passage, so we assumed that this was the prevailing wind direction for our rain event.

4 Results

We first examine the triggering factor-rainfall. Figure 4 shows a (semi)variogram constructed using the rainfall data collected by the 30 gauges (using Huang's definition). The spatial correlation of precipitation among these gauges is not strong. A general trend of increasing variation with increasing distance seems to exist, but has strong irregularities. The RMSE from ordinary kriging (OK) is 84.51 mm and the percent error (PE) is 22.68%. The result was improved slightly by using co-kriging with the DEM, which resulted in a RMSE of 80.52 mm and a PE of 21.61%.

The IDW with $\alpha = 2$ was implemented and the error was found to be slightly higher than that of OK with an RMSE equal to 91.49 mm and PE of 24.56%. The distance decay parameter, α, other than 2, was tested as well. IDW with $\alpha = 3$ yields the highest error (RMSE = 99.98, PE = 26.84) and IDW with $\alpha = 1$ gave the best result among all the selected parameter values (RMSE = 79.76, PE = 21.41).

For the Adaptive inverse distance weighting method (AIDW), a range of distance decay parameter, α, from 0.1 to 3, was used. AIDW outperforms OK, co-kriging, and IDWs with RMSE of 72.66 mm and PE of 19.5%.

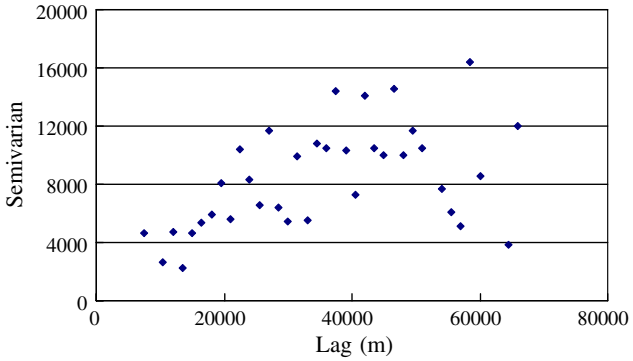

Fig. 4 Semivariogram of the data for the 30 rain gauges

Before using artificial neural network to run the wind-topography model, we examined the azimuthal angle dependency of the semivariogram. Figure 5 shows the directional semivariograms for four hypothetical azimuthal angle intervals. Due to symmetry, directional semivariograms in the North direction were identical to those of the South direction. Figure 5 shows that semivariance of rainfall is relatively small in southeasterly (northwesterly) direction.

We further examine the correlation matrix of each azimuth angle of hypothetical wind flux versus precipitation (results are shown in Table 1 (a) and (b), respectively). Since the correlations are identical but with an opposite sign for directions 180 degrees out of phase, only the results for four directions are shown. Both aspect (Asp) and Exp(0) show high correlation with precipitation with significant P values in the direction of SE (and NW).

With the prevailing southeasterly wind during the typhoon passage, Asp and Exp(0) of SE (or NW) are used as input to the WTNN along with elevation, Z, and SK results. After training the network with 30 rain gauges, the error between predicted values and target values converged and the weights of the connection nodes were obtained. These weights were then used in the interpolation of rainfall over the 9 validation stations.

To demonstrate the utility of the WTNN method, a multi-linear regression (MLR) model was performed. The regression coefficients are shown on Table 2. The MLR RMSE is 84.82 mm and PE is 22.77%.

The RMSE of WTNN is 64.47 mm and PE is 17.31%. Convergence is achieved after about 90 learning cycles. This result is slightly better than that of MLR. We made the

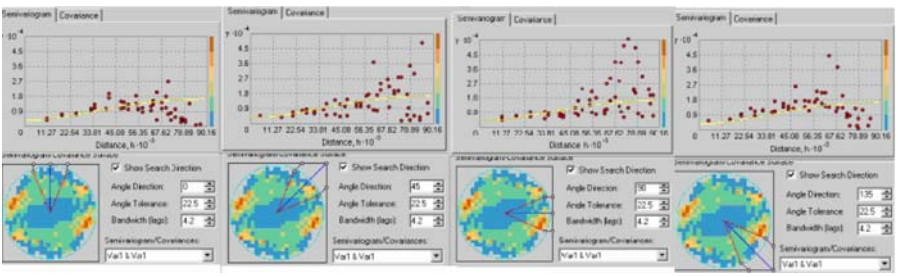

Fig. 5 Directional semivariograms of rain gauges

Table 1 (a) Correlation matrix of Asp to precipitation; (b) Correlation matrix of Exp(0) to precipitation

	N/S	NE/SW	E/W	SE/NW
(a)				
Y (*R* value)	0.332	0.142	0.494	0.490
Y (*P* value)	0.0391	0.3893	0.0014	0.0015
(b)				
Y (*R* value)	0.327	0.025	0.405	0.531
Y (*P* value)	0.0425	0.8795	0.0106	0.0005

Y: Precipitation

Table 2 Coefficients of stepwise regression

Intercept	Z	Asp	Exp(0)
397.013	−0.135	−0.951	−1.046

assumption that this might be caused by low correlation between rainfall and elevation ($R = 0.20$). The correlation value is lower than the range of 0.33–0.83 suggested by Goovaerts (2000) who used monthly data in their study, whereas we use total event rainfall.

We examined the sensitivity of the input parameters to the WTNN results by eliminating parameters one at a time. The best performance was a WTNN without elevation as an input. After eliminating elevation, the RMSE and PE drop to 57.51 mm and 15.44%, respectively. Table 3 summarizes our results.

To perform the simple kriging method, we randomly generated points within a TRMM 2B31 pixel (4 × 4 km) and assigned the rainfall amount collected over a three hour envelope to each point using AIDW. The differences between AIDW and TRMM 2B31 are plotted and a semivariogram diagram was computed before the ordinary kriging processing. The semivariogram closely fits the Gaussian's model as shown in Fig. 6; therefore a reliable prediction is expected. The simple kriging method shows improvement by yielding a RMSE of 2.26 mm and a PE = 17.02%. The performance of SK method depends strongly on the accuracy of the remote sensing information. The more accurate the remote sensing information, the more accurate SK will be. Figure 7 compared results (by percent error) for all methods used in this study.

We next examine the debris-flow susceptibility factors. Fuzzy based factors were obtained from high resolution satellite imagery and a DEM (40 m × 40 m) from Aerial Survey Office of the Forestry Bureau, Taiwan. High resolution satellite imagery data were used to compute percent of vegetation cover (N2 from Eq. 16). GIS was used to process the DEM and obtain slope (N1 from Eq. 15) and area of watersheds (N3 from Eq. 17). A soil map (from the Aerial Survey Office of the Forestry Bureau, Taiwan) was used to determine

Table 3 RMSE and PE of different spatial interpolation techniques

	Kriging	Co-kriging	IDW ($\alpha = 1$)	IDW ($\alpha = 2$)	IDW ($\alpha = 3$)	AIDW	MLR	WTNN	WTNN (W/out Z)
RMSE (mm)	81.51	80.52	79.76	91.49	99.98	72.66	84.82	64.47	57.51
PE (%)	22.68	21.61	21.41	24.56	26.84	19.51	22.77	17.31	15.44

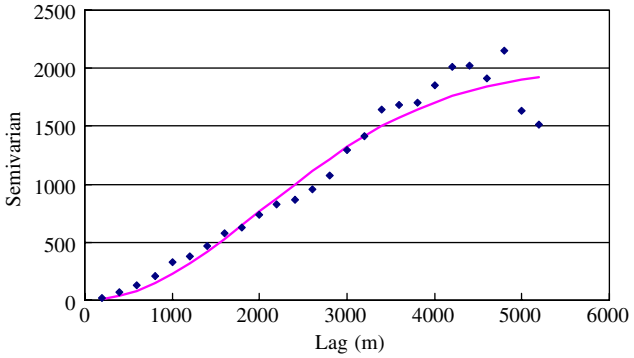

Fig. 6 The semivariogram of simple kriging method

soil properties in each watershed (N4 from Eq. 18). Delineated watersheds and streams in Nan-Tou County are presented in Fig. 8. For cartographic purposes, we use a single point in the downstream area of a watershed to represent a watershed area.

Inputs to self-organizing maps (SOM) are fuzzy based debris-flow susceptibility factors, N1, N2, N3, N4, and rainfall triggering factors-rainfall from the wind-topography (WTNN) model and simple kriging method. Output of SOM is degrees of hazard (DOH). SOM provides great flexibility for decision makers to categorize degrees of risk by simply adding output nodes. Three hazard levels (low, medium and high degrees of hazard) are used as suggested by Soil and Water Conservation Bureau of Taiwan. Among all 187 debris flow watersheds in the study area, 16 watersheds were ranked as low hazard, 135 watersheds as medium hazard, and 36 watersheds as high hazard (Fig. 9). Watersheds were identified by points in the downstream and the degrees of hazard were indicated by the point symbols. All steps in the hazard assessment, including data loading, data analysis and results display, were processed by ArcGIS. A decision maker can easily handle the process using a GIS without dealing with different information systems.

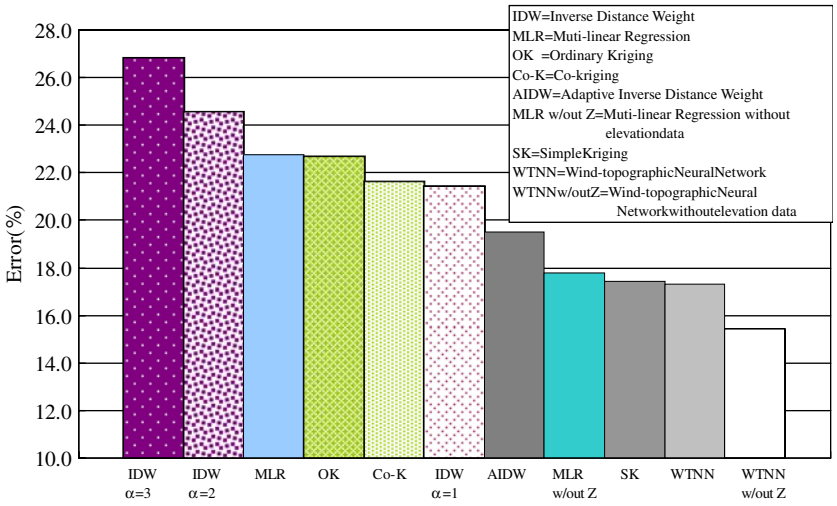

Fig. 7 Percent error of different spatial interpolation techniques

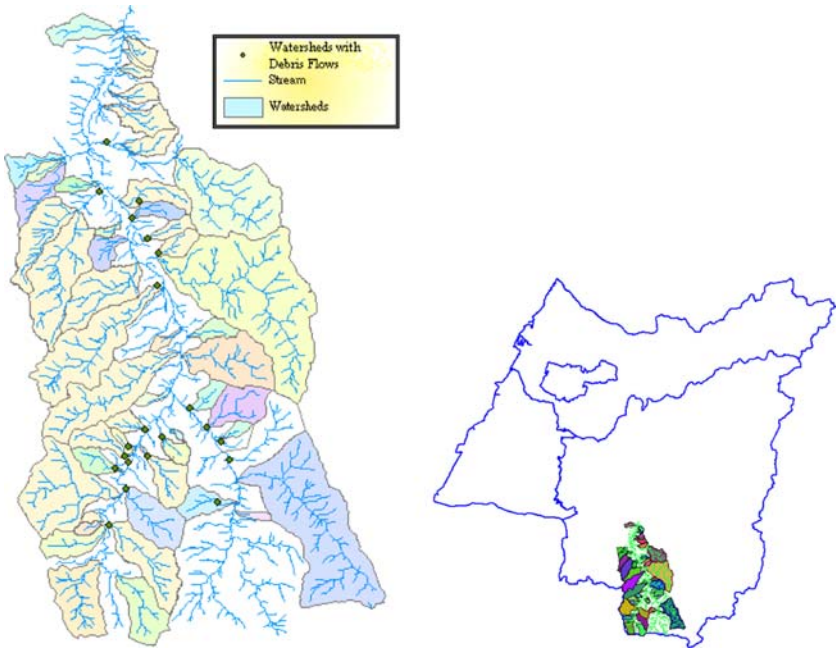

Fig. 8 Delineated watersheds and streams

5 Conclusion and discussion

In order to fully utilize a GIS decision support system for the assessment of rainfall-induced debris flow hazards, we combined watershed characteristics with rainfall estimation based on a 1 km DEM, satellite pixel rainfall estimates (4 km pixels) and large scale wind data. Three spatial interpolation techniques are compared. The AIDW method provides better results than the inverse distance weight method by considering the distribution characteristics of rain gauges and using distance decay parameters. Simple kriging incorporates remote sensing data to minimize the variance between interpolated rainfall values and satellite rainfall data. The wind-topography neural network method integrates the interaction between wind and topography by adapting Antonic's and Legovic (1999) model in an artificial neural network. We demonstrated that the incorporation of topographic and meteorological data outperforms traditional methods such as, kriging, co-kriging, and IDWs. Simple kriging can also improve rainfall estimation by incorporating satellite rainfall information (TRMM 2B31) as local mean values. Among all the methods, the wind-topography neural network method (without elevation information) produced the best results by yielding minimum root mean square and percent errors of RMSE = 57.51 and PE (%) = 15.44% respectively. Since the input variables are generated by a high-resolution DEM (1 km × 1 km), a procedure for interpolating relatively coarse resolution (4 km) satellite rainfall data into high-resolution cells for heavy rainfall events was also demonstrated.

Self-organizing maps that incorporate susceptibility factors (slope, vegetative cover, area of watershed, and soil type) and triggering factors (estimated rainfall by the WTNN model) were used to estimate the hazard of debris flow at low, medium, and high levels.

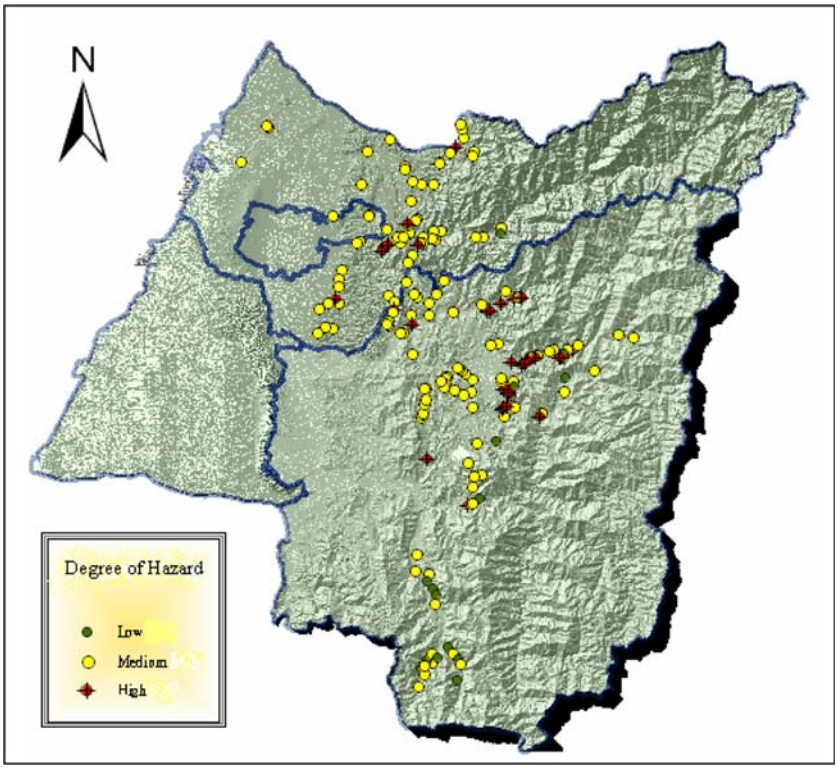

Fig. 9 Map showing different degrees of hazard in the study area

This technique should be further developed for operational, near real-time debris flow warning system.

References

Antonic O, Legovic T (1999) Estimating the direction of an unknown air pollution source using a digital elevation model and a sample of deposition. Ecol Model 124:85–95

Ayalew L, Yamagishi H (2005) The application of GIS-based logistic regression for landslide susceptibility mapping in the Kakuda-Yahiko Mountains, Central Japan. Geomorphology 65(1–2):15–31

Bindlish R, Barros PA (2000) Disaggregation of rainfall for one-way coupling of atmospheric and hydrological models in regions of complex terrain. Global Planetary Change 25(1–2):111–132

Bishop AW (1955) The use of slip circle in the stability analysis of earth slopes. Geotechnique 5(1):7–17

Bishop AW, Morgenstern NR (1960) Stability coefficients for earth slopes. Geotechnique 10(4):129–147

Boots BN, Getis A (1988) Point pattern analysis. Sage Publications, Newbury Park, CA

Borga M, Vizzaccaro A (1997) On the interpolation of hydrologic variables: formal equivalence of multiquadratic surface fitting and kriging. J Hydrol 195:160–171

Burrough PA, McDonnell RA (1998) Principles of geographical information systems, Oxford University Press, Oxford

Casagrande A (1936) Characteristics of cohesionless soils affecting the stability of slopes and earth fills. J Boston Soc Civil Eng 23(1):13– 32

Cheng CZ (2003) Rainfall and geological conditions for debris flow occurrence. Master thesis of National Cheng-Kung University (in Chinese)

Cheng JD, Huang YC, Wu HL, Yeh JL, Chang CH (2005) Hydrometeorological and landuse attributes of debris flows and debris floods during typhoon Toraji, July 29–30, 2001 in central Taiwan. J Hydrol 306(1–4):161–173

Chiu LS, Liu Z, Vongsaard J, Morain S, Budge A, Bales C, Neville P (2006a) Comparison of TRMM and water district rain rates over New Mexico. Adv Atmospheric Sci 23(1):1–13
Chiu L, Shin D-B, Kwiatkowski J (2006b) Surface rain rates from TRMM satellite algorithms. In: Qu SJ et al (eds) Earth system science remote. Springer-Tsinghua University Press
Chon TS, Park YS, Moon KH, Cha EY (1996) Patternizing communities by using an artificial neural network. Ecol Model 90:69–78
Clerici A, Perego S, Telllini C, Vescovi P (2002) A procedure for landslide susceptibility zonation by the conditional analysis method. Geomorphology 48(4):349–364
Daly C, Neilson RP, Philips DL (1994) A statistical topographic model for mapping climatological precipitation over mountainous terrain. J Appl Meteorol 33(2):140–158
Dingman LS (2002) Physical hydrology, 2nd edn. Prentice Hall
Dirks KN, Hay JE, Stow CD, Harris D (1998) High-resolution studies of rainfall on Norfolk Island Part II: Interpolation of rainfall data. J Hydrol 208(1998):187–193
Ermini L, Catani F, Casagli N (2005) Artificial Neural Networks applied to landslide susceptibility assessment. Geomorphology 66:327–343
Gabet EJ, Mudd SM (2005) The mobilization of debris flows from shallow landslides, Geomorphology, Article in process
Giraudel JL, Lek S (2001) A comparison of self-organizing map algorithm and some conventional statistical methods for ecological community ordination. Ecol Model 141:329–339
Goovaerts P (2000) Geostatistical approaches for incorporating elevation into the spatial interpolation of rainfall. J Hydrol 228:113–129
Gómez H, Kavzoglu T (2005) Assessment of shallow landslide susceptibility using artificial neural networks in Jabonosa River Basin, Venezuela. Eng Geol 78(1–2, 5):11–27
Hemmateenejad B, Safarpour MA (2005) Net analyte signal–artificial neuralnetwork (NAS–ANN) model for efficient nonlinear multivariate calibration. Anal Chimica Acta 535:275–285
Hevesi JA, Flint AL, Istok JD (1992) Precipitation estimation in mountainous terrain using multivariant geostatistics. Part II: isohyetal maps. J Appl Meteorol 31:677–688
Hsu K, Gao H, Soroshian S, Gupta H (1997) Precipitation estimation from remotely sensed information using artificial neural networks. J Appl Meteorol 36:1176–1190
Hsu ML, Lu KK (2004) The geomorphic characteristics of debris flows in the 99 peaks area, nantou. J Geograph Sci 38: 1–16 (in Chinese)
Huang TH (2002) Characteristics of rains triggering debris flows in the watershed of chenyoulen stream. Master Thesis of National Cheng-Kung University (in Chinese)
Hürlimann M, Copons R, Altimir J (2006), Detailed debris flow hazard assessment in Andorra: a multidisciplinary approach. Geomorphology 78(3–4):359–372
International Federation of the Red Cross and Red Crescent Societies I (2001) World disasters report 2001
Isaaks EH, Srivastava RM (1989) An introduction to applied geostatistics. Oxford University Press, New York
Jain A, Srinivasulu S (2006) Integrated approach to model decomposed flow hydrograph using artificial neural network and conceptual techniques. J Hydrol 317(3–4, 20):291—306
Jan CD (2000) Introduction to debris flow. Technology Press (in Chinese)
Jakob M, Weatherly H (2003) A hydroclimatic threshold for landslide initiation on the North Shore Mountains of Vancouver, British Columbia. Geomorphology 54(3–4):137–156
Jakob M (2000) The impacts of logging on landslide activity at Clayoquot Sound, British Columbia. CATENA 38(4):279–300
Jiang YC (1998) A study on the judgment of potential debris flows. Master Thesis of National Taiwan University (in Chinese)
Johnson AM (1965) A model for debris flow. Pennsylvania State University unpublished Ph.D. dissertation
Komac M (2006) A landslide susceptibility model using the analytical hierarchy process method and multivariate statistics in perialpine Slovenia. Geomorphology 74(1–4):17–28
Kummerow C, coauthors (2000) The status of the Tropical Rainfall Measuring Mission (TRMM) after two years in orbit. J Appl Meteor 39:1965–1982
Kyriakidis PC, Kim J, Miller NL (2001) Geostatistical mapping of precipitation from rain gauge data using atmospheric and terrain characteristics. J Appl Meteorol 40:1855–1877
Lebel T, Bastin G, Obled C, Creutin JD (1987) On the accuracy of areal rainfall estimation: a case study. Water Res Res 23(11): 2123–2138
Leflaive J, Céréghino R, Danger M, Lacroix G, Loïc TH (2005) Assessment of self-organizing maps to analyze sole-carbon source utilization profiles. J Microbiol Method 62(1):89–102
Levine ER, Kimes DS, Sigillito VG (1996) Classifying soil structure using neural networks. Ecol Model 92:101–108

Lin ML, Jeng FS (2000) Characteristics of hazards induced by extremely heavy rainfall in Central Taiwan—Typhoon Herb. Eng Geol 58:191–207
Lin PS, Lin JY, Hung JH, Yang MD (2002) Assessing debris-flow hazard in a watershed in Taiwan. Eng Geol 66:295–313
Lin CW, Shieh CL, Yuan BD, Shieh YC, Liua SH, Lee SY (2003) Impact of Chi-Chi earthquake on the occurrence of landslides and debris flows: example from the Chenyulan River watershed, Nantou, Taiwan. Eng Geol 71:49–61
Liu YH (2001) The study of spatial characteristics on debris flow in chenyulan creek watershed. Master thesis of National Taiwan University (In Chinese)
Longley PA, Goodchild MT, Maguire DJ, Rhind DW (2001) Geographical information systems and science. Wiley, New York
Luino F (2005) Sequence of instability processes triggered by heavy rainfall in the northern Italy. Geomorphology 66(1–4):13–39
Luk KC, Ball JE, Sharma A (2001) An application of artificial neural networks for rainfall forecasting. Math Comput Model 33(6–7):683–693
Malet JP, Laigle D, Remaître A, Maquaire O (2005) Triggering conditions and mobility of debris flows associated to complex earthflows. Geomorphology 66(1–4): 215–235
Metternicht G, Hurni L, Gogu R (2005) Remote sensing of landslides: an analysis of the potential contribution to geo-spatial systems for hazard assessment in mountainous environments. Remote Sens Environ 98(2–3):284–303
Navone HD, Ceccatto HA (1994) Predicting Indian monsoon rainfall: a neural network approach. Clim Dynam 10: 305–312
Pérez-Magariño S, Ortega-Heras M, González-San José ML, Boger Z (2004) Comparative study of artificial neural network and multivariate methods to classify Spanish DO rose wines. Talanta 62(5, 19):983–990
Philips DL, Dolph J, Marks D (1992) A comparison of geostatistical procedures for spatial analysis of precipitations in mountainous terrain. Agr Forest Meteor 58:119–141
Prudhomme C (1999) Mapping a statistic of extreme rainfall in a mountainous region, Physics and Chemistry of the Earth, Part B: Hydrology. Oceans Atmosphere 24(1–2):79–84
Ramirez MC, Velho HF, Ferreira NJ (2005) Artificial neural network technique for rainfall forecasting applied to the São Paulo region. J Hydrol 301(1–4):146–162
Shakoor A, Smithmyer AJ (2005) An analysis of storm-induced landslides in colluvial soils overlying mudrock sequences, southeastern Ohio, USA. Eng Geol 78(3–4):257–274
Sidle RC, Pearce AJ, O'Loughlin CL (1985) Hillslope stability and land use. Water Resources Monograph 11. Ameican Geophysical Union, 140
Tabios GQ, Salas JD (1985) A comparative analysis of techniques for spatial interpolation of precipitation. Water Res Bull 21(3):365–380
Taylor DW (1937) Stability of earth slopes. J Boston Soc Civil Eng 24:197–246
Thiessen AH (1911) Precipitation averages for large areas. Monthly Weather Rev 39(7):1082–1084
Tobler WR (1970) A computer movie simulating urban growth in the Detroit region. Econ Geography 46(Supplement):234–240
Tseng YC (2004) A composite warning index of rainfall and geological conditions for debris flow. Master thesis of National Cheng-Kung University (in Chinese)
Vanacker V, Vanderschaeghe M, Govers G, Willems E, Poesen J, Deckers J, De Bievre B (2003) Linking hydrological, infinite slope stability and land-use change models through GIS for assessing the impact of deforestation on slope stability in high Andean watersheds. Geomorphology 52(3–4, 16):299–315
Wen BP, Aydin A (2005) Mechanism of a rainfall-induced slide-debris flow: constraints from microstructure of its slip zone. Eng Geol 78(1–2): 69–88
Wong DW, Lee J (2005) Statistical analysis of geographic information with ArcView GIS and ArcGIS. John Wiley & Sons, Inc, Hoboken, NJ